



Investigating the *cis*-regulatory basis of C₃ and C₄ photosynthesis in grasses at single-cell resolution

John Pablo Mendieta^a , Xiaoyu Tu^b , Daiquan Jiang^c , Haidong Yan^a, Xuan Zhang^a , Alexandre P. Marand^{a,1} , Silin Zhong^c , and Robert J. Schmitz^{a,2}

Affiliations are included on p. 11.

Edited by Julia Bailey-Serres, University of California, Riverside, CA; received February 13, 2024; accepted July 23, 2024

While considerable knowledge exists about the enzymes pivotal for C₄ photosynthesis, much less is known about the *cis*-regulation important for specifying their expression in distinct cell types. Here, we use single-cell-indexed ATAC-seq to identify cell-type-specific accessible chromatin regions (ACRs) associated with C₄ enzymes for five different grass species. This study spans four C₄ species, covering three distinct photosynthetic subtypes: *Zea mays* and *Sorghum bicolor* (NADP-dependent malic enzyme), *Panicum miliaceum* (NAD-dependent malic enzyme), *Urochloa fusca* (phosphoenolpyruvate carboxykinase), along with the C₃ outgroup *Oryza sativa*. We studied the *cis*-regulatory landscape of enzymes essential across all C₄ species and those unique to C₄ subtypes, measuring cell-type-specific biases for C₄ enzymes using chromatin accessibility data. Integrating these data with phylogenetics revealed diverse co-option of gene family members between species, showcasing the various paths of C₄ evolution. Besides promoter proximal ACRs, we found that, on average, C₄ genes have two to three distal cell-type-specific ACRs, highlighting the complexity and divergent nature of C₄ evolution. Examining the evolutionary history of these cell-type-specific ACRs revealed a spectrum of conserved and novel ACRs, even among closely related species, indicating ongoing evolution of *cis*-regulation at these C₄ loci. This study illuminates the dynamic and complex nature of *cis*-regulatory elements evolution in C₄ photosynthesis, particularly highlighting the intricate *cis*-regulatory evolution of key loci. Our findings offer a valuable resource for future investigations, potentially aiding in the optimization of C₃ crop performance under changing climatic conditions.

C₄ Photosynthesis | Cis-regulation | Plant Genomics | Regulatory Evolution | Single-cell

Photosynthesis is one of the most critical chemical reactions on the planet whereby CO₂ is metabolized into glucose. Plants have evolved numerous variations of photosynthesis. The most common type of photosynthesis uses the enzyme ribulose 1,5-biphosphate carboxylase oxygenase (RuBisCO) which combines CO₂ with a five-carbon compound ribulose 1,5-biphosphate to create 3-phosphoglyceric acid. This three-carbon compound is then used in a redox reaction within the Calvin Benson cycle, where sucrose is made. The production of this three-carbon compound is what gives this type of photosynthesis, C₃, its name. However, although widely evolved and found in many crop plants, C₃ photosynthesis struggles to perform in hot, arid conditions. In nonideal conditions, O₂ can competitively bind the RuBisCO active site, causing the formation of a toxic intermediate, and reducing photosynthetic efficiency and plant performance (1). Due to increasing temperature caused by anthropogenic climate change, this reduction in photosynthetic capacity for key crop plants poses a major agricultural challenge (2). However, other types of photosynthesis have evolved in hotter conditions and offer a model to potentially alter key C₃ crop plants to be more efficient.

The C₄ photosynthetic pathway is an example of a modified style of photosynthesis that is able to perform in hot conditions. In brief, C₄ typically works by sequestering key photosynthetic enzymes into two different compartments in the leaf made up of different cell types. These two cell types/compartments are bundle sheath (BS) cells, which in C₄ plants generally form a concentric ring around the vasculature, and mesophyll (MS) cells, which make up large portions of the nonvascularized leaf internal cells (3). In the MS, CO₂ is imported and converted to bicarbonate (HCO₃⁻) by the enzyme carbonic anhydrase (CA). Bicarbonate is then converted to a four-carbon molecule oxaloacetate (OAA) by the O₂-insensitive phosphoenolpyruvate carboxylase (PEPC). This OAA molecule made of a four-carbon compound (where C₄ derives its name) is finally converted into a stable metabolite, either malate or aspartate. This intermediate molecule is then transported to the BS where it undergoes a decarboxylation process, by one of three different types of decarboxylases, NAD-dependent malic

Significance

This study advances understanding of the *cis*-regulatory mechanisms underpinning the evolution of C₃ and C₄ photosynthesis in grasses. Leveraging cutting-edge single-cell assay for transposase accessible chromatin-sequencing technology, we reveal intricate cell-type-specific regulatory landscapes that delineate the evolutionary trajectory from C₃ to C₄ photosynthesis. The comprehensive single-cell resolution *cis*-regulatory maps across five grass species, including both C₃ and C₄ types, uncover the dynamic interplay of gene co-option and evolutionary innovation driving this critical adaptation. These findings not only elucidate the genetic foundations of photosynthetic diversity, but also pave the way for future biotechnological approaches to improve crop resilience and efficiency under changing environments.

Author contributions: J.P.M., S.Z., and R.J.S. designed research; J.P.M., X.T., D.J., H.Y., X.Z., and A.P.M. performed research; J.P.M. analyzed data; and J.P.M., S.Z., and R.J.S. wrote the paper.

Competing interest statement: R.J.S. is a co-founder of REquest Genomics, LLC, a company that provides epigenomic services.

This article is a PNAS Direct Submission.

Copyright © 2024 the Author(s). Published by PNAS. This article is distributed under Creative Commons Attribution-NonCommercial-NoDerivatives License 4.0 (CC BY-NC-ND).

¹Present address: Department of Molecular, Cellular, and Development Biology, University of Michigan, Ann Arbor, MI 48109.

²To whom correspondence may be addressed. Email: schmitz@uga.edu.

This article contains supporting information online at <https://www.pnas.org/lookup/suppl/doi:10.1073/pnas.2402781121/-DCSupplemental>.

Published September 23, 2024.

enzyme (NAD-ME), NADP-dependent malic enzyme (NADP-ME), or phosphoenolpyruvate carboxykinase (PEPCK). This decarboxylation reaction releases a CO₂ molecule that enters into the Calvin Benson cycle. The generation and processing of intermediate molecules in cellular compartments allows for concentrated levels of CO₂ to interact with RuBisCO, reducing the inefficiencies mentioned above. Additional types of C₄ photosynthesis have been observed which do not rely on division of metabolites between MS and BS cell types, but instead rely on using dimorphic chloroplast instead as in the species *Bienertia sinuspersici* (4, 5). Current C₄ crops such as maize (*Zea mays*), sorghum (*Sorghum bicolor*), pearl millet (*Cenchrus americanus*), foxtail millet (*Setaria italica*), and broomcorn millet (*Panicum miliaceum*) excel in their ability to operate in adverse conditions.

Although the evolution of C₄ photosynthesis is a complex process, there is tantalizing evidence that engineering C₃ crops to do C₄ photosynthesis might be possible. One piece of evidence that points to this is that C₄ photosynthesis has evolved independently 65 times in different lineages of plants (6). These results indicate that most plant lineages have the genetic material capable of evolving into C₄ photosynthesizers. The *Poaceae* lineage of grasses exemplifies this, as C₄ photosynthesis has evolved independently at least 18 times (7). Interestingly, all of these species use the same core C₄ enzymes and steps, but many use different decarboxylation enzymes as mentioned above (8–10). Furthering this hypothesis is the fact that many C₄-related genes originally evolved from either C₃ photosynthetic genes or key enzymes critical in core metabolism (11, 12). For instance, PEPCK is a key metabolism enzyme in the glycolytic pathways of the Krebs Cycle, with some copies being important in guard cell metabolism (13–15). Instead of novel gene content being the main driver of C₄ photosynthesis, it is more likely due to the correct timing and compartmentalization of key enzymes into specific cell types (16–18). This raises the question of how is gene expression of these key C₄ enzymes regulated. Moreover, as C₄ has evolved multiple times convergently, have similar regulatory networks and paradigms been co-opted to alter when and where these key genes are expressed?

cis-regulatory elements (CREs) are key players in gene regulation, as they both fine-tune expression and provide cell-type specificity (19–22). In brief, these regions operate as binding sites for transcription factors (TFs). TFs are proteins which are able to alter transcription by binding DNA sequences and recruiting transcriptional machinery which can either increase or decrease transcription (23). Thus TFs are able to significantly change molecular phenotypes. Previous work has shown that CREs could be key players in the transition to C₄ photosynthesis. This was demonstrated by taking C₄ genes from *Z. mays* and transforming them into *Oryza sativa*, a C₃ species (24, 25), which revealed that CREs from *Z. mays* genes were able to drive cell-type-specific expression in MS in *O. sativa* (24, 25). Additional analyses have implicated CREs as drivers in the evolution of C₄ photosynthesis. In the genus of plants *Flaveria*, which contains both C₄ and C₃ plants, one key difference in C₄ plants was a specific CRE driving gene expression in MS cells. This 41 bp motif named *Mesophyll expression module 1* is critical for cell-type-specific expression of PEPCK in MS cells, a critical first step in the C₄ pathway (19, 26). Finally, four conserved noncoding sequences were identified to be critical in MS-specific expression of PEPCK in monocots (27). Furthermore, a recent cross-species study examining the binding sites of GLK, a conserved TF regulating photosynthetic genes, revealed that CREs can undergo rapid changes and result in diverse gene expression patterns without the need of altering the TF itself (28). These

findings show that CREs are important genetic elements that plants use for the evolution of C₄ photosynthesis.

Although some CREs critical for cell-type-specific expression of key photosynthetic genes have been identified, they've been restricted to those nearby the transcriptional start sites. This is due, in part, to the challenge of identifying CREs genome wide, as well as limitations in the isolation of BS and MS cells which is labor intensive and challenging. However, a recent study used a multiomic approach in *Z. mays* BS and MS cells and found CREs genome-wide that might be critical in the cell-type-specific regulation of genes (29). One example is the identification of a potential distal CRE ~40 kb upstream of *SULFATE TRANSPORTER4* (*ZmSFP4*), a BS-specific sulfate transporter (29). These results highlight the complexity of identifying loci involved in *cis* regulation. Identifying all CREs associated with C₄ loci is critical in enhancing our understanding of *cis* regulation of key C₄ genes, and would greatly enhance attempts at engineering C₃ crops. During the evolution of C₄ photosynthesis, it is unclear whether these CREs have been preestablished during evolution and co-opted for C₄ photosynthesis or if they evolved independently numerous times. Understanding the ways in which *cis* regulation evolves to control timing and cell-type-specific expression of C₄ photosynthesis genes would greatly assist efforts in engineering C₃ plants to be more C₄-like.

To investigate the role of CREs and their potential contribution in controlling key C₄ genes, we used single-cell indexed assay for transposase accessible chromatin sequencing (sciATAC-seq) to identify cell-type-specific CREs from five grass species representing diverse C₄ subtypes, as well as an additional C₃ outgroup. We investigated the cell-type specificity of both the core C₄ enzymes, and those which are unique to each photosynthetic subtype. Further, we identify CREs of C₄ genes and find cell-type-specific CREs that might be critical in C₄ gene expression. We find that some of these regulatory regions appear not just conserved in a single C₄ subtype, but in all of the C₄ species we studied. Finally, we leverage these data to find TF binding motifs enriched in MS and BS cell types and use these motifs to catalog these regulatory loci.

Results

Identification and Annotation of Cell Types in Diverse Species.

To investigate CREs in BS and MS cells potentially important in C₄ photosynthesis, we generated replicated sciATAC-seq libraries for four different C₄ species, comprising three different C₄ subtypes NADP-ME (*Z. mays*, *S. bicolor*), NAD-ME (*P. miliaceum*), and PEPCK (*Urochloa fusca*), and a C₃ outgroup species (*O. sativa*) (Fig. 1A). Libraries were filtered for high-quality cells by first pseudobulking the sciATAC-seq libraries, and identifying accessible chromatin regions (ACRs). Using these ACRs, per nucleus quality metrics were then calculated such as fraction of reads in peaks, transcriptional start site enrichment, and total integration events per nucleus (*Methods*). Nuclei found to have a high proportion of organellar reads were also removed, with values being adjusted on a per library basis (*Methods*). Clustering of cells was done on genomic bins, and with additional cells removed that had a high correlation with *in silico* generated doublets, and clusters were removed that were skewed toward one replicate by greater than 75% (*Methods*). After filtering on per nucleus quality metrics, we identified 16,060 nuclei in *Z. mays*, 15,301 nuclei in *S. bicolor*, 7,081 nuclei in *P. miliaceum*, 19,110 nuclei in *U. fusca*, and 5,952 nuclei in *O. sativa* (*SI Appendix*, Fig. S1 and Dataset S1).

Due to variation in genome size and content, cell-type annotation for each dataset was done independently using the reference

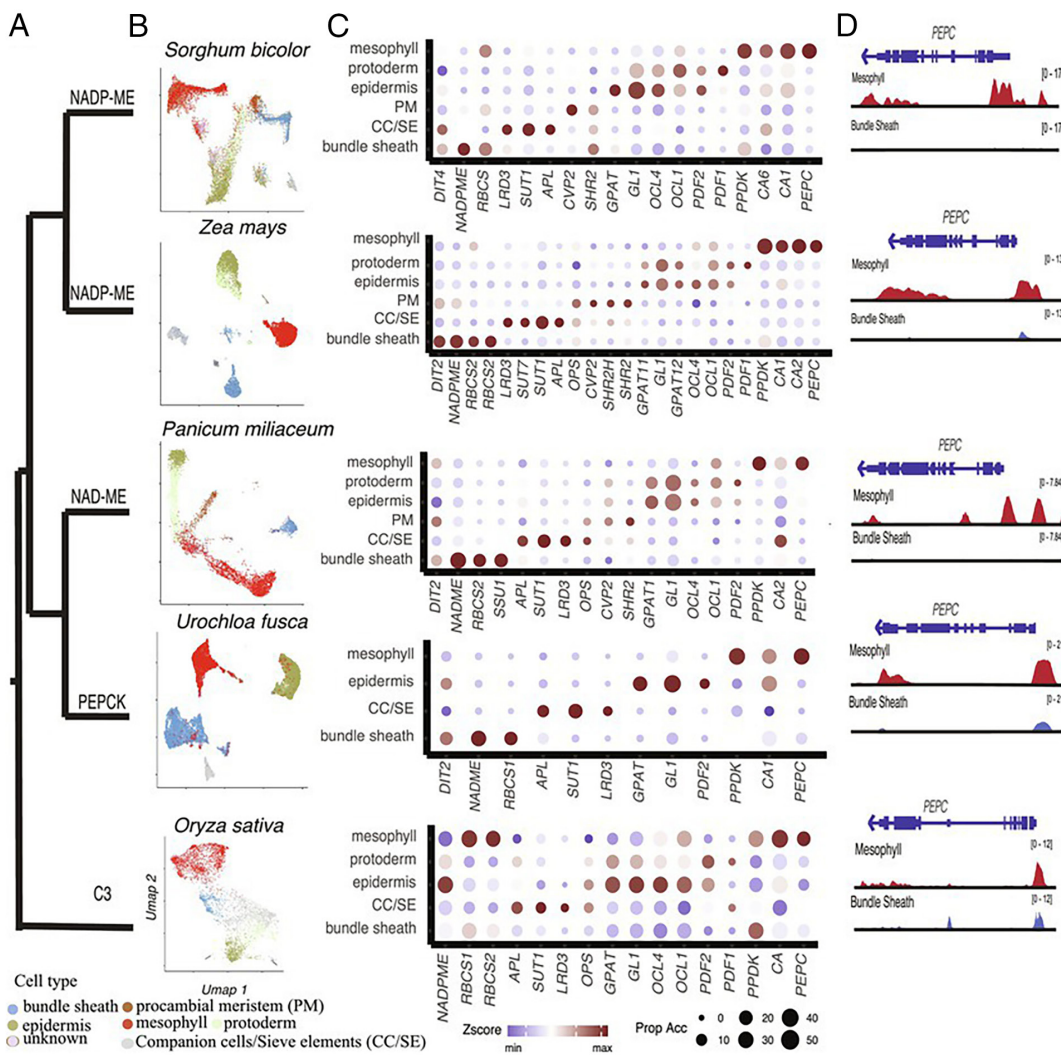


Fig. 1. Annotation of cell types in diverse grass species at single-cell resolution. (A) A phylogeny indicating the relationship of various C₃ and C₄ photosynthesizers sampled. In this sample, two NADP-ME subtypes are represented, one NAD-ME subtype, a PEPCK subtype, as well as a C₃ species. (B) UMAP embedding showing the annotation for each species. A cell type legend is below. (C) Dotplots for various marker genes used to annotate each species. The y axis represents cell types, and the x axis is a list marker genes used to annotate different cell types. The size of each circle is proportional to the number of cells within that cell type that showed chromatin accessibility of the marker. Color is z-score transformed values across clusters of gene chromatin accessibility across the clusters. (D) Screenshots of the PEPC locus for all sampled species. For each screenshot, the top track shows the protein coding, the red track is chromatin accessibility of MS cells, and the blue track is the chromatin accessibility of BS cells.

genome for each species (Fig. 1B). We used multiple approaches to annotate cell types. Orthologs of key marker genes from *Z. mays* and *O. sativa* were identified using a phylogenetics-based approach (Methods). This allowed for the identification of marker genes for specific cell types in a cross-species context. To gauge gene activity of these marker genes, gene body chromatin accessibility was used as a proxy for expression (Fig. 1D) (21, 30). Cell-type annotation was done manually taking into consideration marker gene chromatin accessibility, marker enrichment in clusters, as well as ontological relationships between cell types (SI Appendix, Figs. S2–S19). Due to the lack of marker genes for many cell types in plants, as well as the challenge of annotating a broad sample of species, we reduced resolution of our annotation across our datasets to ensure accurate comparisons between variable species (Fig. 1B). All markers used to annotate cell types in this manuscript can be found in Dataset S2.

Deeper exploration of the list of marker genes from *Z. mays* showed conservation of gene body chromatin accessibility in markers for certain cell types (Datasets S2 and S3). As expected, for the C₄ plants, RIBULOSE BISPHOSPHATE CARBOXYLASE SMALL SUBUNIT1 (*RBCS1*) and RIBULOSE BISPHOSPHATE

*CARBOXYLASE SMALL SUBUNIT2 (*RBCS2*)* were enriched in BS cells compared to MS cells (Fig. 1C), a pattern that was not found in *O. sativa*. Additionally, *PEPC1* showed MS-specific chromatin accessibility in all of the C₄ species sampled (Fig. 1D). Additionally, we found conservation of marker genes like *SUCROSE TRANSPORTER 1 (*SUT1*)* in companion cells and sieve elements, and *GLOSSY1 (*GL1*)* in epidermis cells, indicating that these historically described marker genes are likely important in this diverse set of species. This analysis provides an examination of core-C₄ marker genes' chromatin accessibility across a diverse sample of plant species at cell-type resolution.

Chromatin Accessibility of Core C₄ Enzymes Shows Similar Cell-Type Bias, but Differing Evolutionary Origins. We measured the chromatin accessibility bias of the C₄-associated enzymes. Due to the diverse nature of the plants sampled, and the C₄ photosynthetic subtypes, we separated enzymes into core- and subtype-specific groups. This list comprised nine core C₄ enzymes, and nine variable enzymes. These enzymes were assigned to one of these two groups based on if they are found in all C₄ subtypes (core) or are specific to only one or two subtypes (variable). One

example of a core enzyme is carbonic anhydrase, which is used to generate bicarbonate from CO_2 , as well as for the regeneration of phosphoenolpyruvate from oxaloacetate in the BS cells by means of PEPCK (Fig. 2A). The list of gene families that we considered as core or variable is found in [Dataset S3](#).

To investigate the cell-type bias of these enzymes, we used chromatin accessibility of the gene (gene body as well as 500 bp upstream of the transcriptional start site) (Fig. 2B). Cell-type bias was calculated as the \log_2 fold change of BS/MS chromatin accessibility. In order to identify core C_4 enzymes across these species, we used OrthoFinder, named and numbered the enzyme models based off of their relatedness to *Z. mays* copies of known core C_4 genes (31). Using only cell-type-specific chromatin accessibility data, we observed expected cell-type bias with many orthologs of the maize MS-specific core C_4 genes showing MS-specific bias as compared to BS (Fig. 2C). For instance, in all C_4 species, PEPCK, which regenerates PEP from OAA in BS cells, always showed a BS-specific bias (Fig. 2A and C). Additionally, PEPC, which converts bicarbonate to OAA in MS cells, showed MS-specific bias for all species sampled, except the C_3 outgroup *O. sativa* (Fig. 2A and C). These results highlight the quality of the data and the cell-type annotations for these single-cell datasets.

When analyzing these data in tandem with the phylogenetic trees, we noticed that some of the key enzymes showed different cell-type specificity based on their evolutionary origin ([SI Appendix, Figs. S21 and S22](#)). For instance, for carbonic anhydrase in *P. miliaceum*, the orthologs that showed the largest bias between MS and BS cell types were not the copies that were the most evolutionary closely related to the *Z. mays* and *S. bicolor* cell-type-specific copies (Here *PmCA1* and *PmCA2*). Rather, a copy found in a separate clade (*PmCA3*) showed the most MS-specific bias (Fig. 2C). This indicates that

during the evolution of C_4 , different sets of carbonic anhydrases were likely co-opted. One challenge using chromatin accessibility in this context, however, is the fact that neighboring gene models can occlude cell-type-specific signals. For instance, in the *S. bicolor* copy of *RBCS1*, a BS-specific gene has a neighboring gene model directly upstream which shares a promoter region making measurement of the cell-type-specific bias of some loci challenging when using chromatin accessibility data ([SI Appendix, Fig. S23](#)).

One unexpected result from this analysis was the lack of cell-type-specific bias for *MALATE PHOSPHATE ANTIPORT 1 (DIC1)*, also known as *DICARBOXYLATE/TRICARBOXYLATE TRANSPORTER 1 (DTC1)* in *Z. mays*. It has been previously reported that *DIC1* had BS-specific expression bias in *Z. mays* as well as in *P. miliaceum* (32–34). However, there is not a clear signal based on the chromatin accessibility data. This could indicate that some ACRs harbor multiple CREs active in different cell types that are not obvious in chromatin accessibility data or that the cell-type-specificity observed is not due to *cis*-regulation, possibly involving posttranscriptional processes (Fig. 2C). Last, as expected, there was very little bias in the C_3 outgroup (*O. sativa*). In total, 12/13 of the core C_4 enzymes showed cell-type-specific bias in *Z. mays*, 7/12 in *S. bicolor*, 16/21 in *P. miliaceum*, 11/13 in *U. fusca*, and finally 0/16 in *O. sativa*. These data demonstrate that chromatin-accessibility data can be leveraged to investigate the cell-type regulation of C_4 genes while also taking into consideration their evolutionary relationships in a cross-species context.

Key C_4 Subtype Genes Show Potential Convergent Evolution in Cell-Type-Specific Bias. We investigated the variable enzymes that give each C_4 subtype its unique properties by focusing on two species (*S. bicolor* and *Z. mays*) from the *NADP-ME*

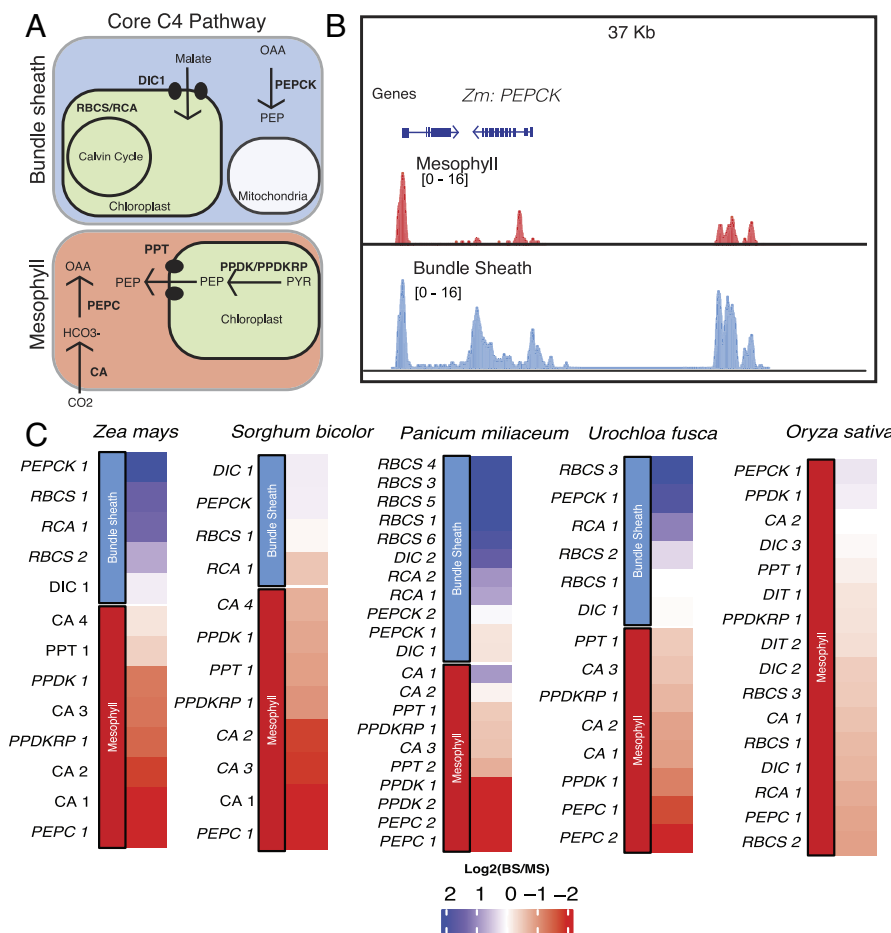


Fig. 2. Cell-type chromatin-accessibility bias for core enzymes in C_4 and C_3 species. (A) Schematic of the core C_4 enzymatic pathway. Core C_4 enzymes are defined as those which maintain their cell-type-specificity in all C_4 subtypes sampled. The red and blue squares represent MS and BS cells, respectively. Enzymes are labeled in bold, and transporters are denoted by shapes. Intermediate molecules are indicated by nonbolded text. (B) Screenshot of *PEPCK* in *Z. mays*. Blue tracks correspond to BS chromatin accessibility and red tracks show MS chromatin accessibility. Tracks are equally scaled to facilitate comparison. (C) Heatmaps of chromatin accessibility bias of the core C_4 enzymes. Values within each heatmap correspond to $\text{Log}_2(\text{BS}/\text{MS})$. Blue indicates increased BS chromatin accessibility and red indicates increased MS chromatin accessibility. Each species column and subtype was clustered independently, and genes were assigned as being MS- or BS-specific (top/bottom of heatmap) based on literature. Enzyme copies were distinguished phylogenetically.

subtype (Fig. 3A). As expected, chromatin accessibility bias was observed for enzymes previously reported as having cell-type-specific expression patterns, similarly to the core C₄ enzyme set (29, 35). Reassuringly, one of the most biased enzymes identified was NADP-ME, the key enzyme of the redox step in NADP-ME subtypes. More specifically, of the multiple copies of NADP-ME that exist in *Z. mays*, we observed the expected cell-type bias for the known BS-specific copy, ME3, a key factor in C₄ (here *ZmNADP-ME1*) (Fig. 3B). We noticed in *S. bicolor*, the BS-specific NADP-ME and the MS-specific NADP-malate dehydrogenase (NADP-MDH) gene copies are recent tandem duplications, each maintaining their respective cell-type specific chromatin accessibility (Fig. 3B and C and SI Appendix, Figs. S22 and S23). The malate transporters DICARBOXYLIC ACID TRANSPORTER1/2 (*DIT1/2*) also demonstrated their expected cell-type-specific bias with *DIT1* being MS specific and *DIT2* being BS specific in both species (Fig. 3B and C). However, upon

further inspection of the phylogenies of the *DITs* in *S. bicolor*, we noticed a pattern where the most BS-biased copy, *SbDIT4* (Sobic.004G035500), was phylogenetically more closely related to the *ZmDIT1*. Something which has been previously reported (33, 36). These results indicate that over evolutionary time, even members of the same C₄ photosynthetic subtype, which likely share a C₄ ancestor, can use different paralogous loci to achieve cell-type-specific expression. This highlights that C₄ evolution is an ongoing process.

NAD-ME subtypes in *P. miliaceum* are interesting, as the intermediate molecule being passed between MS and BS does not take the form of malate, but instead aspartate, alanine, and oxaloacetate (Fig. 3D). At least one gene copy of all the key redox enzymes, NAD-ME and the NAD-dependent malate dehydrogenase (NAD-MDH), show BS-biased chromatin accessibility (Fig. 3E and F). Interestingly, of the three copies of NAD-MDH analyzed, only two showed bias for BS. Next, we evaluated two key enzymes

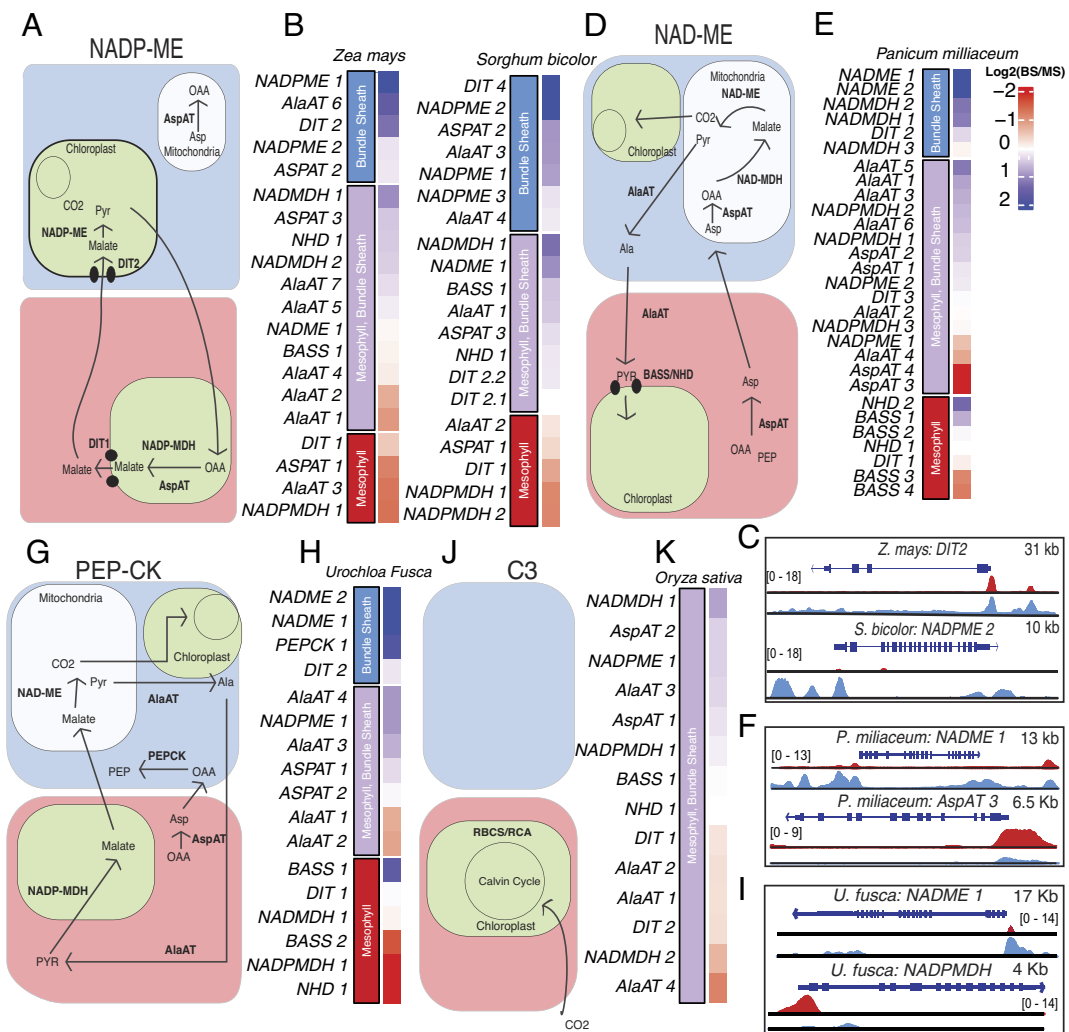


Fig. 3. Cell-type chromatin accessibility bias for variable C₄ genes associated with C₄ subtypes. (A) Schematic of C₄ enzymatic pathways for various NADP-ME subtypes. The red and blue squares represent MS and BS cells. Enzymes are labeled in bold, and transporters are denoted by shapes. Intermediate molecules are indicated by nonbolded text. For clarity, core enzymes have been removed. (B) Heatmaps of chromatin accessibility bias in C₄ NADP-ME subtypes. Values within the heatmap correspond to Log2(BS/MS). Blue indicates increased BS-chromatin accessibility and red indicates increased MS-chromatin accessibility. Genes were labeled as being BS specific (blue), BS/MS specific (purple), or MS specific (red) based on previous literature. (C) Screenshot of various C₄ subtype enzymes and their chromatin accessibility profiles around the TSS. Blue tracks correspond to BS chromatin accessibility, and red tracks show MS chromatin accessibility. Tracks are equally scaled to facilitate comparison. (D) Additional schematic diagrams corresponding to specific C₄ subtypes, with enzymes and transporters identified similarly to (A). (E) Heatmaps showing chromatin accessibility bias for the corresponding C₄ subtypes, following the same format as (B). (F) Additional chromatin accessibility profiles as in (C), aligned with the relevant subtypes. (G) Additional schematic diagrams corresponding to specific C₄ subtypes, with enzymes and transporters identified similarly to (A). (H) Heatmaps showing chromatin accessibility bias for the corresponding C₄ subtypes, following the same format as (B). (I) Additional schematic diagrams corresponding to specific C₄ subtypes, with enzymes and transporters identified similarly to (A). (J) Heatmaps showing chromatin accessibility bias for the corresponding C₄ subtypes, following the same format as (B). (K) Heatmaps showing chromatin accessibility profiles around the TSS for various C₄ subtypes. (L) Additional chromatin accessibility profiles as in (C), aligned with the relevant subtypes. (M) Additional schematic diagrams corresponding to specific C₄ subtypes, following the same format as (B).

associated with the generation of critical intermediate metabolites, Aspartate aminotransferase (AspAT), and Alanine aminotransferase (AlaAT). It has been reported that some AspAT have cell-type-specific expression patterns, with the MS-specific copy of the protein being transported to the cytosol and the BS-specific copy being transported to the mitochondria (Fig. 3 E and F) (37–39). Of the four copies of AspAT we examined, two (*PmAspAT3/4*) showed significant MS-specific bias, whereas the other two copies (*PmAspAT1/2*) did not show significant deviation toward BS (Fig. 3E). This possibly indicates differing levels of regulation for the AspAT copies that did not show the expected BS bias, or missing copies of AspAT that we have not investigated. Within AlaAT, however, we identified one copy, *PmAlaAT1*, showing MS-specific bias, and *PmAlaAT6* showing BS-specific bias; something that has been previously hypothesized based on biochemical information (40). Additionally, somewhat unexpectedly is that we did not observe clear bias for sodium bile acid symporters (*BASS*) and sodium:hydrogen antiporters (*NHD*) (Fig. 3E). These two proteins together form a functioning sodium bile acid symporter system, which balances the ratio of sodium and is important in the transport of pyruvate into the chloroplast of MS cells (41). Although two copies of the *BASS* genes were MS biased, only a single copy of *NHD* was slightly MS biased. Surprisingly, we do observe slight cell-type-specific chromatin accessibility bias for malate transporter *DIT1/DIT2* in *P. miliaceum*. This is somewhat surprising, as malate is not the main 4-carbon intermediate used by NAD-ME subtypes (10). This highlights the flexible nature of *P. miliaceum* in terms of its C₄ photosynthetic style, as it has been implicated that it can perform some of the metabolite shuttling as the NADP-ME subtype (10, 42, 43). The potential flexibility of *P. miliaceum* in its style of C₄ makes it an extremely interesting species to study, especially when considering that it does not share common C₄ ancestry with *Z. mays* or *S. bicolor*. This lack of evolutionary relationship between *P. miliaceum* and *S. bicolor* and *Z. mays* makes the comparison between *P. miliaceum* and its closer relative *U. fusca* all the more valuable. These observations point to the complicated nature of some of these C₄ photosynthetic subtypes. While the obvious subtype-specific enzymes show expected chromatin-accessibility bias, others do not.

Using the *PEPCK* subtype in *U. fusca*, we evaluated cell-type bias of enzymes that operate as an intermediate between NAD-ME and NADP-ME subtypes (Fig. 3G). Copies of *NAD-ME* and *PEPCK* showed significant BS bias (Fig. 3 H and I). Additionally, *NADP-MDH* was significantly biased toward MS, reflecting its critical role in the regeneration of malate from pyruvate (Fig. 3H). We also observed one copy of *BASS*, which was heavily MS biased, as well as the only copy of *NHD* being highly MS biased (Fig. 3G) (44). Within the *BASS* family, based on the phylogenies, it appears one clade of *BASS* genes was co-opted to be MS specific, whereas the other clade remained somewhat BS specific. This potentially indicates that this co-opted clade may have been predisposed for C₄ photosynthesis at the common ancestor of *P. miliaceum* and *U. fusca*. Additionally, we also find one MS-biased and one BS-biased version of AlaAT (Fig. 3H).

Finally, when evaluating genes in the C₃ outgroup *O. sativa*, we only observed significant chromatin accessibility bias for three of the 14 enzymes. This is expected given the overall lack of enzymatic bias seen in C₃ species (Fig. 3K). Interestingly though, we did find a single instance where one copy of *AspAT* is BS specific, suggesting that this copy of *AspAT* might slowly be co-opted into being more BS-specific (Fig. 3K). Even more interesting is the slight BS-specific bias of the rice *NAD-MDH*, a BS-specific enzyme in the NAD-ME subtypes. These results show a series of complex evolutionary relationships where many different genes

can be co-opted into the C₄ pathway and highlight the myriad ways in which C₄ evolution occurs.

Cell-Type-Specific ACRs of Both Core- and Subtype-Specific Enzymes. Although measuring the gene body chromatin accessibility of C₄ enzymes is valuable, it does not inform us about the cell-type-specific *cis*-regulatory environment controlling these genes, as we only included 500 bp upstream in this initial analysis. To identify all potential CREs important for regulation of C₄ enzymes, we identified cell-type-specific ACRs using a modified entropy metric (Methods; *SI Appendix*, Figs. S36 and S37). In short, cell-type-specific ACRs are those which are unique to either a single cell-type or two or three cell types in contrast to broadly accessible ACRs which are accessible in many different cell types. For each C₄ enzyme, in both the core and the noncore set, we identified ACRs around them. We only considered ACRs to be potential regulators of a locus based on distance, with assigned ACRs needing to be less than 200 kb away from the target enzyme, and requiring that no other gene intervenes between the ACR and enzyme in question. In total, across all variable and core enzymes and taking into consideration only C₄ species, we find that on average, C₄ genes have between 2 and 3 cell-type-specific ACRs, with an additional 2 to 3 broadly accessible ACRs (Fig. 4A and Dataset S5).

For all C₄ subtypes, the key redox enzymes all showed BS cell-type-specific ACRs, potentially identifying critical CREs for proper cell-type-specific expression. For instance, in *Z. mays*, *NADP-ME1* had five BS-specific ACRs, in *S. bicolor*, *NADP-ME2* had five BS-specific ACRs, in *P. miliaceum*, *NAD-ME1* had four BS-specific ACRs, and in *U. fusca*, *PEPCK*, had three BS-specific ACRs (Fig. 4 A and C). Additionally, of the MS-specific enzymes, we consistently observed numerous cell-type-specific ACRs around the carbonic anhydrase family. On average, there were 3.5 MS-specific ACRs for each copy of carbonic anhydrase across all of the species. This likely reflects the fact that carbonic anhydrase is critical in the initial steps of C₄, and also important in CO₂ sensing (45). We also noticed an intriguing pattern where enzymes which were accessible in one cell type had cell-type-specific ACRs of the other cell type. For instance, around *RBCS2*, a BS-specific enzyme, we found a series of MS-specific ACRs (Fig. 4D). On average, we found 2.5 BS-specific ACRs around *RBCS* and 1.5 MS-specific ACRs. This contrasting pattern was observed in key photosynthetic enzymes in all of the C₄ subtypes. This likely indicates that some of these ACRs contain CREs that negatively regulate *RBCS* in MS, as cell-type-specific CRE usage has been implicated as being an important driver in proper compartmentalization (46, 47). The identification of ACRs around key C₄ enzymes provides a detailed map about potential *cis*-regulators of these loci, which provides the basis for future investigation into the direct function of each of these ACRs and how they might be altering transcription in multiple different ways. These results show that there are likely multiple ACRs important to cell-type specificity of these enzymes.

Traditionally, the field has focused on *cis*-regulation within a set distance from the transcriptional start site, often 1 to 2 kb, which is thought to generally encompass the promoter (48). However, we observed abundant distal cell-type-specific ACRs for many of these key genes (Fig. 4B). For instance, the average distance of an ACR to its C₄ enzyme is 10,080 bp (*Z. mays*), 3,017 bp (*S. bicolor*), 4,260 bp (*P. miliaceum*), 2,358 bp (*U. fusca*), and 4,730 bp (*O. sativa*), indicating that the *cis*-regulatory space for these enzymes is far greater than previously appreciated, where a majority of the focus in the literature is on putative promoters.

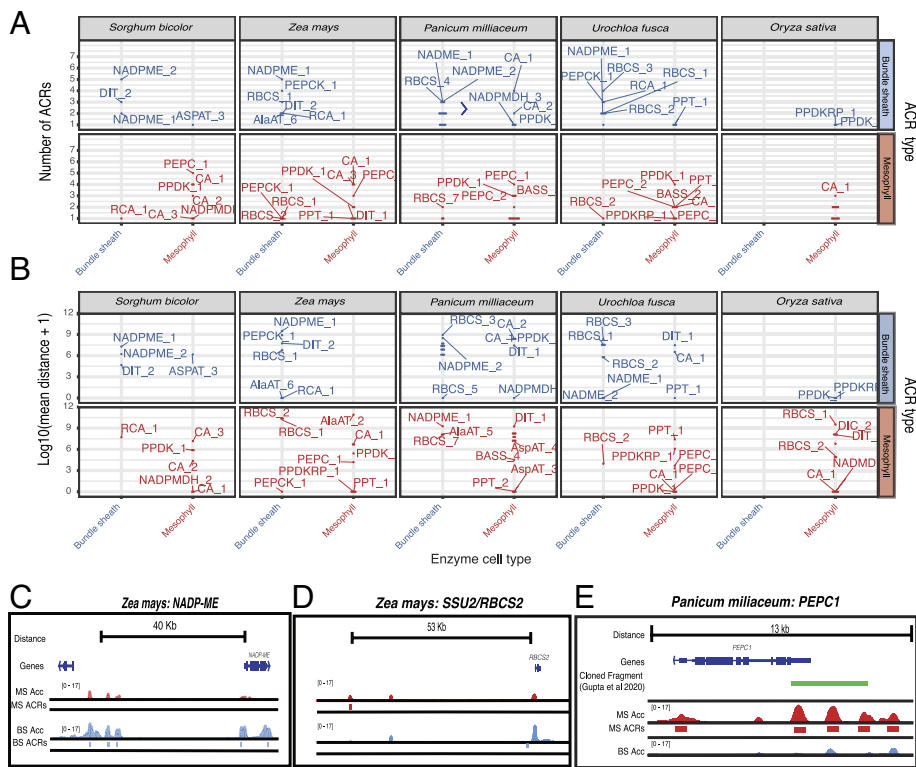


Fig. 4. Investigating the number and distance of cell-type-specific ACRs around C₄ enzymes across subtypes. (A) Dot plots showing the number of cell-type-specific ACRs around each enzyme. The x axis indicates which cell type these enzymes are found in. The y axis is counts of ACRs. The graph is further subdivided with the *Top* panel being broad ACRs, *Middle* panel BS-specific ACRs, and the *Bottom* being MS-specific ACRs. Enzymes are labeled. (B) Dotplots showing the mean distance of cell-type-specific ACRs to their closest C₄ enzyme. The x axis indicates which cell type these enzymes are found in. The x axis is the genomic distance to the C₄ enzyme in question. If an enzyme had multiple cell-type-specific ACRs, the distance was averaged (mean). (C) Screenshot of NADP-ME1 in *Z. mays*. Blue tracks correspond to BS chromatin accessibility and red tracks show MS chromatin accessibility. Tracks are equally scaled to facilitate comparison. All genes found within this window are shown. (D) Screenshot of RBCS2 in *Z. mays*. Blue tracks correspond to BS chromatin accessibility and red tracks show MS chromatin accessibility. Tracks are equally scaled to facilitate comparison. All genes found within this window are shown. (E) Screenshot of PEPC1 in *P. milaceum*. The green fragment represents the cloned promoter from Gupta et al. (27), which was identified by minimap2 alignment. Blue tracks correspond to BS chromatin accessibility and red tracks show MS chromatin accessibility. Tracks are equally scaled to facilitate comparisons.

To test this, we compared the identified ACRs to a series of previously reported cloned promoters. We found that for *Z. mays* and *S. bicolor* the ACR space identified includes significantly more regions that are distal to their target gene (*SI Appendix*, Fig. S25C and Dataset S6) (25, 49, 50).

The genome of *Z. mays* emphasizes this point, as the subtype-specific enzyme *NADP-ME* has three cell-type-specific BS ACRs distal to the transcriptional start site, with the furthest being 34,336 bp away (Fig. 4C). These distal ACRs provide critical regulatory loci to further investigate. Interestingly, we found some enzyme/ACR pairs with opposite cell-type-specificity (i.e., BS-specific enzyme, MS-specific ACR). Many of these ACRs were distally located. For example, in *Z. mays*, the MS-specific ACR of *RBCS* was 36,171 bp upstream (Fig. 4D). When investigating ACRs around promoters, we were struck at how often cell-type-specific ACRs occurred outside of the bounds of previously analyzed promoters. For example, in *PEPC* in *P. miliaceum*, a recent analysis demonstrated that a series of conserved noncoding sequences found between species were able to drive MS expression (27). When we looked at chromatin accessibility data of the promoter fragment which was cloned from *PEPC*, we identified many MS-specific ACRs within the cloned fragment, but an additional one upstream. This result shows the advantage of using scATAC-seq data to identify candidate CREs for certain genes, removing the guesswork of cloning fragments to investigate and providing a detailed cell-type-specific regulatory map of the locus (Fig. 4E). Thus, scATAC-seq greatly improves the search space of the active CREs potentially driving cell-type-specific gene expression patterns.

The Evolutionary Relationships of ACRs Associated with C₄ Genes

Are Complex and Variable. Next, we explored the evolutionary histories of these ACRs. Due to the fact that the C₄ subtypes come from different radiation events, (with *Z. mays* and *S. bicolor* likely sharing a C₄ ancestor and *U. fusca* and *P. miliaceum* sharing a different C₄ ancestor), we were curious to evaluate whether a

majority of the ACR space around these genes were either novel, or shared among these species. We implemented a pairwise sequence-based approach by identifying sequence conservation of ACRs between the study species using BLAST (*SI Appendix, Supplemental Methods*). The majority of important C₄ genes have both novel and conserved ACRs. For example, PPDK, a MS-specific enzyme, shares ~25% of its ACRs across all species examined including the *O. sativa* C₃ outgroup (Fig. 5A). Interestingly, RUBISCO ACTIVASE (RCA), a critical enzyme in photosynthesis which removes inhibitory molecules from the RuBisCO active site, had novel ACRs in all the C₄ species examined, whereas RCA in the C₃ species *O. sativa* shared one ACR with all the C₄ species. This might indicate that each of the C₄ species gained regulatory sequences at RCA or that *O. sativa* might have lost them (Fig. 5A). Focusing on NADP-ME revealed notable divergence in its associated ACRs, even among closely related species. For example, in *Z. mays*, two out of nine ACRs linked to NADP-ME1 were unique, lacking counterparts in other species (Fig. 5A). This is particularly striking given that *S. bicolor*, belonging to the same C₄ subtype, diverged from *Z. mays* only 13 mya (51). Similarly, in *S. bicolor*, the BS-specific NADP-ME2 variant exhibited two out of five unique ACRs. This pattern underscores the rapid and distinct evolutionary trajectories of ACRs in C₄ plants. A full list of gene families, and gene models, and their relative conservation is found in *SI Appendix, Fig. S26A*. Using this same approach to study all of the core class of C₄ enzymes did not reveal a generalizable pattern associated with gain or loss of ACRs around C₄ genes (*SI Appendix, Fig. S26A*). Our findings not only confirm the dynamic evolution of *cis*-regulatory sequences in C₄ enzymes but also align with existing research that highlights rapid *cis*-regulatory changes among closely related species (48, 52).

While investigating the ACRs around the C_4 genes is interesting, understanding how cell-type specificity is achieved across C_4 subtypes is needed for efforts to engineer C_4 photosynthesis. When looking at just the cell-type-specific ACRs around key C_4 loci, we find a similar pattern where there is a mix of both conserved and novel ACRs. For example, we found that some of the MS-specific

ACRs associated with *PPDK* and *PEPC* are highly conserved in all of the studied species. Interestingly, the MS-specific ACRs around *PEPC* were only found in the C₄ species, and not in the C₃ outgroup, *O. sativa* (Fig. 5B). This indicates that some of the CREs that allow *PEPC* expression in MS likely evolved after the split between the most recent common ancestors. We also observed that *NADP-ME* possessed numerous BS-specific ACRs that were conserved in all species, including *O. sativa* (Fig. 5B). Considering proper compartmentalization of *NADP-ME* in BS cells is only critical in two of the three C₄ subtypes, this was surprising. However, in both *S. bicolor* and *Z. mays*, there were novel BS-specific ACRs associated with each key *NADP-ME*. In *Z. mays*, one out of the five BS-specific ACRs was novel to *Z. mays*, and in *S. bicolor* two out of the five were novel to *S. bicolor*. Upon inspection of all the *NADP-ME* loci in genome browsers, we were struck by the complexities and shuffling that occurred at these BS cell-type-specific ACRs (Fig. 5C). These results highlight that extensive *cis*-regulatory evolution is occurring in each of these species, and on a cell-type-specific level. Additionally, this may point to the fact that the novel BS-specific ACRs found in *S. bicolor* and *Z. mays* may be more important for proper BS-specific expression than the conserved regulatory elements.

Although binary classification of ACRs was useful to decipher larger scale patterns between key enzymes, we next tested whether larger segments of sequence were conserved around some C₄ genes as compared to others. We profiled the relative amount of conserved sequence at each of these ACRs, as alignment of sequence between species gives greater resolution about important ACRs. One interesting observation from this analysis was the fact that the cell-type-specific ACRs around *PEPC* appear to be novel between *Z. mays* and *U. fusca* (Fig. 5D and *SI Appendix*, Figs. S26–S31). This suggests that these regulatory loci emerged independently, and

yet are still likely important in cell-type-specific expression of *PEPC*. Additionally, around the *NADP-ME* loci in *P. miliaceum*, we found diverse evolutionary histories with both copies *NADP-ME1* and *NADP-ME2* having both conserved and novel BS-specific ACRs (one out of four ACRs were novel for *NADP-ME1*, and zero out of the two were conserved for *NADP-ME2*) (Fig. 5D). The ACRs from *NADP-ME1* are conserved in *U. fusca*, whereas all three BS-specific ACRs are conserved in relation to *P. miliaceum*. Pointing to the fact that the ACRs have likely maintained their cell-type specificity, and are likely critical drivers in the correct expression of *NADP-ME* loci. These results highlight the dynamic evolution of cell-type-specific ACRs around key C₄ loci, and that even closely related subtypes have evolved novel ACRs potentially critical in terms of proper gene expression, as well as compartmentalization.

Identification of De Novo TF-Binding Motifs from Cell-Type-Specific Chromatin Data Reveals Rapid Sequence Diversification of ACRs.

Leveraging the cell-type-resolved datasets, we identified de novo cell-type-specific TF motifs in BS and MS ACRs (Fig. 6A and B; *Methods*; and *SI Appendix*, Fig. S32). We selected the BS-specific motifs based on motif similarity within C₄ species for BS, and motif similarity seen across all species for MS. Additionally for the identification of BS-specific motifs, we identified motifs which did not appear to have a corresponding motif in *O. sativa* (*SI Appendix, Supplemental Methods*). Reassuringly, within the BS-specific motifs, we identified a DOF TF motif, which is a key driver in the switch to C₄ photosynthesis (29, 53, 54). In brief, the DOF TFs have been implicated as being potential drivers of proper gene expression in *Z. mays* C₄ genes, both as repressors and activators. For example, *ZmDOF30* has been implicated as being important in driving BS-specific gene expression (29, 53, 54). In total, we identified three BS-specific motifs, and four MS-specific de novo motifs that are shared between the species

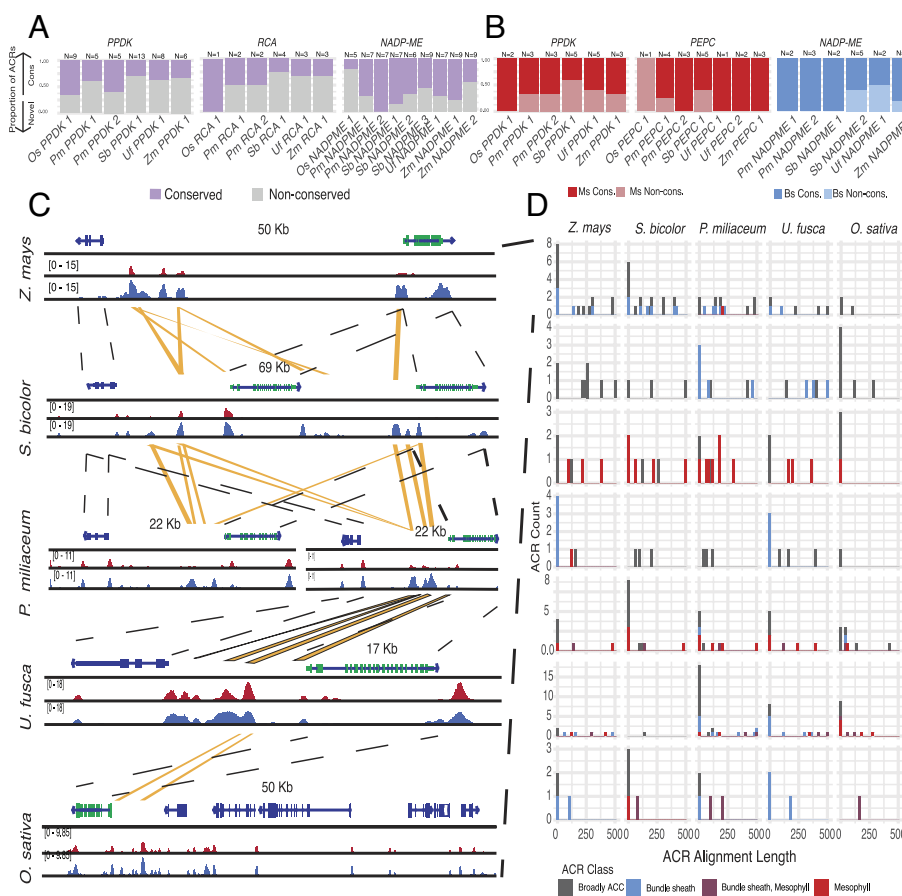


Fig. 5. The evolutionary relationships of *cis*-regulatory regions around C₄ genes are complex, being composed of both novel and conserved ACRs. (A) The proportion of all ACRs that are conserved or novel for the following gene families *PPDK*, *RCA*, and *NADP-ME*. Purple bars represent ACRs that have any sequence aligned to them from a different species, and gray represents ACRs where sequences are not alignable. The number of ACRs in each locus is labeled at the top of each column. (B) The proportion of cell-type-specific ACRs that are conserved and novel for the following gene families, *PPDK*, *PEPC*, and *NADP-ME*. Red bars only consider MS-specific ACRs, and blue bars only consider BS-specific ACRs. (C) Screenshot of the conservation of BS-specific ACRs around *NADP-ME* across species. From top to bottom, the species are *Z. mays*, *S. bicolor*, *P. miliaceum*, *U. fusca*, and *O. sativa*. *NADP-ME* is annotated in green for all species. Dashed bars between gene models represent the same gene model, and yellow bars are conserved ACRs. Browser tracks are blue for BS, and red for MS. Browser tracks are scaled within each species to allow for direct comparisons. (D) The length of ACRs that are conserved in a cross-species context. Rows represent gene families, and columns represent species. Each histogram is the number of ACRs within the loci of that gene family. The x axis is the length of the ACR that is conserved and the y axis is the count. ACRs are color coded according to the legend.

sampled (Fig. 6 A and B and *SI Appendix*, Fig. S32). Using motif comparison tools, we were able to assign five out of the six motifs to a putative TF family, implicating potential novel regulators in BS-and MS-specific gene expression (*SI Appendix, Supplemental Methods* and Fig. S29). We surveyed the C₄ ACRs for the presence and absence of these motifs to determine whether they provide the information needed for cell-type specificity. We additionally overlaid our BLAST results from the previous analysis in order to explore the relationship between these motifs and conservation (Fig. 6C). A substantial number of motifs were present within the nonconserved regions of the ACRs. For instance, in one MS-specific ACR associated with *ZmCA3* 12/13 MS-specific motifs were found in nonconserved regions, suggesting these regions could be critical for driving the cell-type-specificity of this locus (Fig. 6D).

We expanded the analysis of BS- and MS-specific motifs in conserved and nonconserved regions of ACRs across key loci in the C₄ species. On average the MS-specific motifs are more conserved than the BS-specific motifs (Fig. 6 E and F and *SI Appendix*, Fig. S33 A). Agreeing with previous models of C₄ evolution where some motifs that are MS specific have been co-opted to operate in C₄ photosynthesis (Fig. 6D) (11). Interestingly, we noticed a pattern where around PPDK, many of the MS-specific motifs appeared to be in nonconserved sequences for all of our species sampled (*SI Appendix*, Fig. S33 A and B). This pattern is further highlighted in both NADPME, and NADME loci, where a majority of the BS-specific motifs occurred in nonconserved ACRs for NADPME. This pattern is more nuanced in the NADME ACRs, as *P. miliaceum* and *U. fusca* share a significant amount of conserved sequence containing BS-specific motifs in the ACRs, suggesting that the BS-specific regulatory changes associated with these motifs are important (*SI Appendix*, Fig. S33A). These results highlight the capacity of genome-wide single-cell *cis*-regulatory maps to pinpoint key TF motifs important for the evolution of cell-type specificity.

The DITs in the NADP-ME Subtypes Demonstrate Dynamic CRE Evolution. Upon analyzing the malate transporters DICARBOXYLIC ACID TRANSPORTERS (*DITs* also known as the *DCTs*), we noticed the DITs in the NADP-ME subtypes showed an interesting pattern where the copies of *DIT1* in *Z. mays* and *S. bicolor* showed MS-specific chromatin accessibility, but the BS-specific copies of the *DITs* showed a more complex evolutionary history (Fig. 3B and *SI Appendix*, Fig. S34). We generated a phylogeny with additional species and found that the BS-specific copy of *ZmDIT2* is related to two additional copies of *DITs* which are not BS-specific in *S. bicolor*

(Here *SbDIT2.2* and *SbDIT2.1*) (*SI Appendix*, Fig. S34). *S. bicolor* has a BS-specific copy of *SbDIT4*, which shares a clade with *ZmDIT1*. These results are consistent with earlier studies that found similar patterns and gene expression profiles of these copies of the *DITs* in *Z. mays* and *S. bicolor* (33, 36, 55). Although previous studies have documented changes in cell-type-specific gene expression for the BS-specific copies of the *DITs*, the mechanisms underlying these changes remain unclear. By using cell-type-specific ACRs, we explored whether expression changes are associated with changes in the number of cell-type-specific cis-regulatory elements over evolutionary time.

To understand how cell-type specificity changed in these *DITs* due to changes in *cis*-regulation, we compared the ACRs associated with the *DITs*, and mapped the TF-binding motifs found within each ACR (*Methods*). For the MS-specific *DIT1s*, we focused on a MS-specific ACR located at the 3' end of *DIT1* in *Z. mays* (*SI Appendix*, Fig. S34). Upon comparing this ACR to *S. bicolor*, we were struck that the sequence found in the *Z. mays* ACR was actually split in two in *S. bicolor*, neither of which demonstrated cell-type specificity in *S. bicolor* (*SI Appendix*, Fig. S34). A closer inspection of motifs in these ACRs showed many MS-specific motifs (*SI Appendix*, Fig. S34). These motifs might promote MS-specific gene expression of this locus. However, many *S. bicolor* MS-specific ACRs were not found in regions with any homology to *Z. mays* (*SI Appendix*, Fig. S34). These results point to the rapid change of candidate CREs (cCREs) in this locus, and likely indicate that cCREs important in cell-type-specific gene expression might not be only found in conserved regulatory regions (56). Rather, selection of MS-specific gene expression is ongoing and may yield significantly different regulatory environments in relatively short evolutionary time scales.

Next, we examined the BS-specific *ZmDIT2* and its two orthologs *SbDIT2.1* and *SbDIT2.2*, which are not BS specific (*SI Appendix*, Fig. S35). The BS-specific ACR around *ZmDIT2* has many DOF TF motifs (*SI Appendix*, Fig. S35). These motifs are interesting, as expression changes within the DOF TF family could be important in driving BS-specific gene expression in C₄ plants (29, 53, 57). When comparing the BS-specific ACRs around *ZmDIT4* to the more closely related copies of *SbDIT2.1* and *SbDIT2.2*, we found no conservation of these DOF TF motifs, and rather a significant lack of BS-specific TF motifs (*SI Appendix*, Fig. S35). Since neither of these *DIT* copies in *S. bicolor* show BS-specific expression, this result makes sense. Potentially providing a model where the *ZmDIT2* locus either gained these cCREs allowing for this copy of *ZmDIT2* to have BS-specific gene expression, or *S. bicolor* lost these BS-specific motifs, and had a gain in *SbDIT4* specificity. In either scenario,

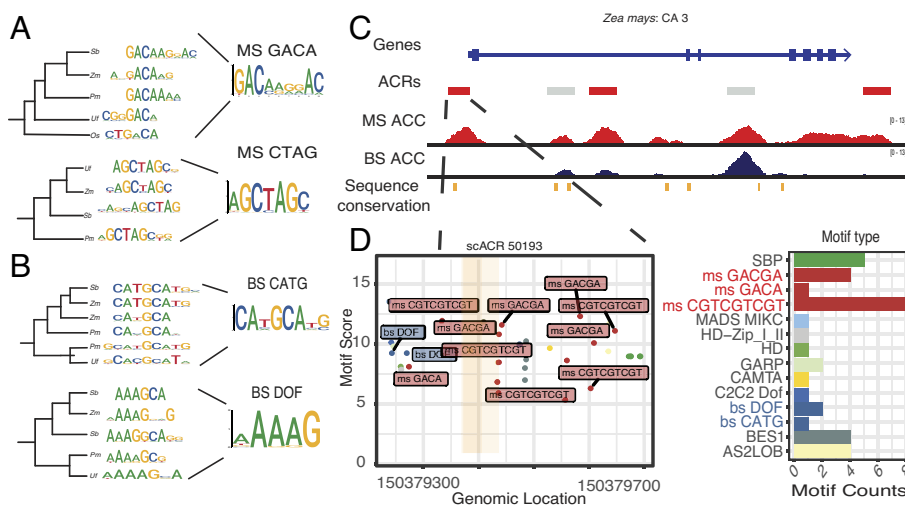


Fig. 6. Identification of cell-type-specific TF motifs reveals a complex relationship between sequence conservation and motif presence. A subsample of MS- (A) and BS-specific (B) de novo TF motifs identified. (Left) De novo motifs were clustered by the correlation of their PWMs and a correlation-based tree was generated. (Right) Representative PWMs identified through de novo analysis. (C) Screenshot of the *ZmCA3* locus. ACRs are color coded based on their cell-type specificity. MS- and BS-chromatin accessibility tracks are equally scaled for comparison. Sequence conservation is identified by the ACR having sequence homology to other CA ACRs from a different species. (D) An example of the conservation and motif landscape of one MS-specific ACR at *ZmCA3*. Left, the location of the motifs in ACRs with MS- and BS-specific motifs labeled. Orange highlighted regions correspond to the region of sequence conservation seen above. Right, quantification of the motifs found in the ACR. The X axis is the motif count, and the Y axis is the motif.

it demonstrates the rapid pace of CRE evolution, and how these regions might be altering cell-type-specific gene expression. These results contrast with *SbDIT4*, where the ACRs around this locus are BS specific, and contain BS-specific motifs identified in our previous analysis (*SI Appendix*, Fig. S35). In total, these results highlight the rapid rate of regulatory change around key C₄ loci, and highlight the fact that there are likely key regulatory switches outside of conserved sequences. Finally, these results emphasize the fast pace in which cell-type specificity changes in plants

Discussion

Understanding the evolution of *cis*-regulation associated with C₄ photosynthesis has been a long-standing goal in the field of plant biology. In this study, we demonstrated the utility of single-cell ATAC-seq data to investigate many aspects of the evolution of C₄ photosynthesis. By identifying cell-type-specific chromatin accessibility from four C₄ species composed of three different C₄ subtypes, as well as a single C₃ outgroup, we were able to compare key genes and their ACRs which define and distinguish C₄ photosynthesis. We have shown that by using gene-body chromatin accessibility data, we can measure cell-type-specific bias of both core, and subtype-specific C₄ enzymes. When considering the gene family trees of many of these genes, we show diverse co-option of loci into the C₄ pathway. Additionally, we identify cell-type-specific ACRs surrounding these key C₄ enzymes. We find numerous cell-type-specific ACRs surrounding key C₄ enzymes, many of which fall outside of the core promoter region. Additionally we find that around all of the C₄ enzymes there is a mix of both conserved and novel cell-type-specific ACRs indicating that regulatory evolution of these regions is ongoing. Finally, we use cell-type-specific ACRs to identify a series of de novo binding motifs which appear to be cell-type specific, and show that these motifs surround C₄ loci, and have a mixed relationship with conservation depending on the motif. This indicates that cell-type-specific TF motifs are rapidly changing around C₄ loci.

Investigation of the CREs driving cell-type-specific expression of C₄ genes is challenging. This often requires evaluation using transgenic plants, which limits the number of CREs that can be tested. This has greatly hampered efforts at understanding how *cis*-regulation of C₄ genes evolves, whether by co-option of existing CREs or emergence of new ones. Our results show the complex nature of CRE evolution of C₄ genes, including those specific to C₄ subtypes. While we observe conservation of ACRs around many C₄ genes, we do see interesting examples where the subtype-specific enzymes have evolved novel ACRs (*NAD-MEs* in *P. miliaceum*, and *PEPCK* in *U. fusca*). These results support that there is likely a combination of both co-opting preexisting CREs, as well as evolving new ones to facilitate proper expression and cell-type-specification of genes. This is further exemplified by the analysis of the *DIT* family of transporters, where we show striking accumulation of cell-type-specific TF motifs in non-conserved regions of ACRs between two closely related species. This highlights that the regions of the genome promoting cell-type-specific gene expression are likely found in both conserved, and novel regions. Another recent single-cell genomic study of the evolution of CREs important for photosynthesis using a comparison between *O. sativa* and *S. bicolor* reached similar conclusions (57). They frequently found different ACRs and TF motifs in promoters of orthologous C₄ genes (57). Future efforts to assay these candidate CREs using reporter assays, transgenesis, and genome editing will be required. Additionally, expanding these analyses outward to all genes associated with photosynthesis might provide valuable insights into how genes in the Calvin-Benson cycle alter their regulation in their adaptation to C₄ photosynthesis. Fortunately, these high-resolution

maps of cell-type-specific ACRs of these key genes/species provide a strong foundation to build upon.

Although these studies provide a blueprint for the study of key candidate CREs associated with C₄ loci, profiling cell-type-specific chromatin accessibility of additional species would be greatly beneficial. Although *O. sativa* is an invaluable outgroup for this study, additional more closely related C₃ species might make these comparisons simpler, and add additional resolution. For instance the C₃ grass species *Dichanthelium oligosanthes* is more closely related to *U. fusca* and *P. miliaceum* and has a recently completed reference genome (58). Adding more species would enable greater resolution in the comparison of cell-type-specific ACRs, as the genetic distance between the species we examined, and *O. sativa* make identification of conserved and novel ACRs challenging. As an example, the ACRs associated with *NAD-MEs* in *P. miliaceum* might be co-opted instead of novel, however, based on our sampling, we cannot say.

Genome editing analysis of many of these ACRs would significantly advance which ACRs, and more specifically which CREs within the ACRs are most important for cell-type-specific expression (22). However, currently generating genome edits in monocots is challenging, time consuming, and expensive. Fortunately, improvements to transgenesis are constantly improving making achieving these goals more likely in the future (59). It is also important to consider that mutational analysis of CREs is not straightforward, often requiring numerous editing events of the *cis*-regulatory landscape of each gene. Previous studies have shown that deletions of many CREs produce variable molecular and morphological phenotypes, further complicating our understanding of the *cis*-regulatory code (60–62). And finally, many species, including *P. miliaceum* and *U. fusca* have to date never been transformed. This highlights the need to continually improve transgenesis methods to help facilitate the molecular dissection of CRE. In conclusion, this study provides a comprehensive map of cell-type-specific ACRs around key C₄ genes, which reveals the dynamic evolution and diversity of *cis*-regulation of C₄ genes.

Methods

Plant Growth Conditions and Sampling. Seedlings of all five plant species, including maize (*Z. mays* B73), sorghum (*S. bicolor* BTx623), proso millet (*P. miliaceum* L. CGRIS 00000390), and browntop signalgrass (*U. fusca* LBJWC-52), along with the C₃ plant rice (*O. sativa* Nipponbare), were grown under the conditions of 12:12 Light/Dark cycles at 30 °C Light/22 °C Dark and at 50% humidity. The sampling of the C₄ species was timed to coincide with a specific developmental stage, identified when the ligule of the third leaf became visible, marking the third leaf unfolding, yet prior to the appearance of the fourth leaf. For the C₃ species, rice, 18-d-old leaves were used to correspond with the equivalent stage of the C₄ species.

Library Preparation. Nuclei isolation for the experiments was conducted using fresh seedlings of both the C₄ and C₃ species at their respective developmental stages. The methodology for nuclei extraction, encompassing the buffer composition and the subsequent steps, was used with procedures outlined for single-nucleus combinatorial indexing with transposed-based ATAC-seq library construction, as detailed in a prior study (63).

Barcode Correction Read Alignment and Mapping of Tn5 Insertions. Read UMIs were processed using cutadapt (version 4.5) to identify UMIs (64). First, the index adapter sequences were trimmed from the reads. Next, the well barcodes and Tn5 barcode within the reads were identified, removed from the original sequencing read, and appended to the read header. Reads were aligned using BWA (version 0.7.17) (65). Reads were filtered using samtools (version 1.16.1) for mapping quality of >10 for *Z. mays*, *S. bicolor*, *U. fusca*, and *O. sativa*. *P. miliaceum* required a greater threshold of 30 given its recent whole genome duplication (66). Duplicate reads were removed using picard tools (version 2.25.0) (67). Single-base pair Tn5 integration events were mapped using the python script makeTn5bed.py. Finally, for each barcode only unique Tn5 integration sites were used.

Isolating High-Quality Cells. Cells were filtered using Socrates (21). In short, Fraction of Reads in Peaks (FRIP) scores were calculated for each cell by pseudobulking the libraries and identifying peaks. For each individual cell, FRIP score, TSS, enrichment, as well as correlation to background were used to isolate high-quality cells. Additional details can be found in *SI Appendix, Supplemental Methods*.

UMAP embeddings were then calculated for each species utilizing genomic bins (68). Additional bin selection criteria and clustering specifics can be found in *SI Appendix, Supplemental Methods*. Doublets were then removed using the in silico approach Scrublet (69) (*SI Appendix, Supplemental Methods*). Harmony (version 0.1.1) was used to adjust replicate overlap with parameters “theta = 2, nclust = 4, and var = sampleID” (70). After integration, clusters which skewed greater than 75% toward one replicate were removed from downstream analysis.

Annotation of Cell Types. Cell types were annotated by calculating gene chromatin accessibility for marker genes in each genome on a per-cell basis. These values were then visualized on the UMAP embedding, and clusters with numerous marker genes associated with the same cell-type were used as evidence. Additionally, for each louvain cluster, enrichment of marker genes was calculated by comparing the cluster average as compared to a random shuffle of random cells. The top five most enriched markers were used in tandem with the UMAPs to ascertain cell-type identity. We also tested the statistical significance of the marker gene using Presto, a modified Wilcoxon rank-sum test in order to identify the most unique marker gene in each cluster (71). Additional methods implemented to ensure comparison of the same cell types can be found in Supplemental methods.

Identifying Cell-Type-Specific ACRs. To identify cell-type specific ACRs, a modified bootstrapping method was used which drew inspiration from the modified entropy metrics found in ref. 72. On a per ACR basis, Tn5 integrations per cell-type were summed and counts per million (CPM) normalized. These values were then converted to a probability by using the following equation (below, Eq. 1). From this probability statement, a modified Shannon entropy metric was calculated, followed by a metric of specificity *Qpt*. For robust cell-type-specific ACR identification, the annotated cell-type was bootstrapped 5,000 times. To generate the null distribution of specificity scores, individual cell annotations were scrambled to generate an equal number of null cell-type classifications. For each null value, the entropy and specificity score were calculated. Finally, a nonparametric approach was used to identify how many

of the real bootstraps fell outside of the null distribution using a one-tailed test. ACRs specific to greater than three were classified as broadly accessible, less than or equal to three as cell type restricted, and a single cell-type as cell-type specific. Additional details can be found in Supplemental methods.

$$pi = \frac{qi}{\sum(qi)}, \quad [1]$$

$$Hp = -\sum pi \log_2(pi), \quad [2]$$

$$Qpt = Hp - \log_2(pt). \quad [3]$$

Data, Materials, and Software Availability. sciATAC-seq data for *Z. mays*, *S. bicolor*, *U. fusca*, and *P. miliaceum* is found in NCBI under the following bioproject PRJNA1063172 (73). Leaf data for *O. sativa* can be found under the following SRR bioproject PRJNA100757 (74). All scripts used for processing and analyzing data in this manuscript can be found at the following GitHub repository: https://github.com/Jome0169/Mendieta.C4_manuscript (75). Additionally, all datasets with both MS- and BS-specific accessibility profiles, their ACRs, as well as their BLASTN relationships can be found on the epigenome browser <https://epigenome.genetics.uga.edu/PlantEpigenome> (76). All datasets can be found under the subfolder Mendieta_et_al.C4_project.

ACKNOWLEDGMENTS. This research was funded by awards from the NSF (IOS-2134912 and IOS-1856627) and the Office of Research to R.J.S. and Hong Kong University Grant Council (GRF 1409420) to S.Z. A.P.M. and J.P.M. were supported by the NIH (K99GM144742) and (T32GM142623), respectively. This research was additionally funded with support from the National Natural Science Foundation of China (32100438 & 32370247) and Shanghai Jiao Tong University 2030 Initiative (to X.T.).

Author affiliations: ^aDepartment of Genetics, University of Georgia, Athens, GA 30605; ^bShanghai Collaborative Innovation Center of Agri-Seeds, Joint Center for Single-Cell Biology, School of Agriculture and Biology, Shanghai Jiao Tong University, Shanghai 200240, China; and ^cState Key Laboratory of Agrobiotechnology, School of Life Sciences, The Chinese University of Hong Kong, Hong Kong, SAR

1. G. Bowes, W. L. Ogren, R. H. Hageman, Phosphoglycolate production catalyzed by ribulose diphosphate carboxylase. *Biochem. Biophys. Res. Commun.* **45**, 716–722 (1971).
2. T. Wheeler, J. von Braun, Climate change impacts on global food security. *Science* **341**, 508–513 (2013).
3. M. D. Hatch, C4 photosynthesis: A unique blend of modified biochemistry, anatomy and ultrastructure. *Biochim. Biophys. Acta (BBA), Rev. Bioenerg.* **895**, 81–106 (1987).
4. S. Offermann, T. W. Okita, G. E. Edwards, Resolving the compartmentation and function of C4 photosynthesis in the single-cell C4 species *Bienertia sinuspersici*. *Plant Physiol.* **155**, 1612–1628 (2011).
5. H. Akhani et al., *Bienertia sinuspersici* (Chenopodiaceae): A new species from Southwest Asia and discovery of a third terrestrial C4 plant without Kranz anatomy. *Syst. Bot.* **30**, 290–301 (2005).
6. R. F. Sage, A portrait of the C4 photosynthetic family on the 50th anniversary of its discovery: Species number, evolutionary lineages, and Hall of Fame. *J. Exp. Bot.* **67**, 4039–4056 (2016).
7. R. F. Sage, P. A. Christin, E. J. Edwards, The C4 plant lineages of planet Earth. *J. Exp. Bot.* **62**, 3155–3169 (2011).
8. U. Gowik, P. Westhoff, The path from C3 to C4 photosynthesis. *Plant Physiol.* **155**, 56–63 (2011).
9. Grass Phylogeny Working Group II, New grass phylogeny resolves deep evolutionary relationships and discovers C4 origins. *New Phytol.* **193**, 304–312 (2012).
10. X. Rao, R. A. Dixon, The differences between NAD-ME and NADP-ME subtypes of C4 photosynthesis: More than decarboxylating enzymes. *Front. Plant Sci.* **7**, 01525 (2016).
11. K. Kajala et al., Multiple *Arabidopsis* genes primed for recruitment into C4 photosynthesis. *Plant J.* **69**, 47–56 (2012).
12. J. Sheen, C4 gene expression. *Annu. Rev. Plant Physiol. Plant Mol. Biol.* **50**, 187–217 (1999).
13. R. Chollet, J. Vidal, M. H. O’Leary, Phosphoenolpyruvate carboxylase: A ubiquitous, highly regulated enzyme in plants. *Annu. Rev. Plant Physiol. Plant Mol. Biol.* **47**, 273–298 (1996).
14. M. H. O’Leary, Phosphoenolpyruvate carboxylase: An enzymologist’s view. *Annu. Rev. Plant Physiol.* **33**, 297–315 (1982).
15. W. H. Outlaw Jr., Kinetic properties of guard-cell phosphoenolpyruvate carboxylase. *Biochem. Physiol. Pflanz.* **186**, 317–325 (1990).
16. M. Matsuoka, T. Numazawa, Cis-acting elements in the pyruvate, orthophosphate dikinase gene from maize. *Mol. Gen. Genet.* **228**, 143–152 (1991).
17. M. S. Ku et al., High-level expression of maize phosphoenolpyruvate carboxylase in transgenic rice plants. *Nat. Biotechnol.* **17**, 76–80 (1999).
18. M. Nomura et al., The evolution of C4 plants: Acquisition of cis-regulatory sequences in the promoter of C4-type pyruvate, orthophosphate dikinase gene. *Plant J.* **22**, 211–221 (2000).
19. U. Gowik et al., Cis-regulatory elements for mesophyll-specific gene expression in the C4 plant *Flaveria trinervia*, the promoter of the C4 phosphoenolpyruvate carboxylase gene. *Plant Cell* **16**, 1077–1090 (2004).
20. E. D. Kim et al., Dynamic chromatin accessibility deploys heterotypic cis/trans-acting factors driving stomatal cell-fate commitment. *Nat. Plants* **8**, 1453–1466 (2022).
21. A. P. Marand, Z. Chen, A. Gallavotti, R. J. Schmitz, A cis-regulatory atlas in maize at single-cell resolution. *Cell* **184**, 3041–3055.e21 (2021).
22. F. Meng et al., Genomic editing of intronic enhancers unveils their role in fine-tuning tissue-specific gene expression in *Arabidopsis thaliana*. *Plant Cell* **33**, 1997–2014 (2021).
23. F. Spitz, E. E. M. Furlong, Transcription factors: From enhancer binding to developmental control. *Nat. Rev. Genet.* **13**, 613–626 (2012).
24. M. Matsuoka, J. Kyozuka, K. Shimamoto, Y. Kano-Murakami, The promoters of two carboxylases in a C4 plant (maize) direct cell-specific, light-regulated expression in a C3 plant (rice). *Plant J.* **6**, 311–319 (1994).
25. M. Matsuoka, Y. Tada, T. Fujimura, Y. Kano-Murakami, Tissue-specific light-regulated expression directed by the promoter of a C4 gene, maize pyruvate, orthophosphate dikinase, in a C3 plant, rice. *Proc. Natl. Acad. Sci. U.S.A.* **90**, 9586–9590 (1993).
26. U. Gowik et al., A MEM1-like motif directs mesophyll cell-specific expression of the gene encoding the C4 carbonic anhydrase in *Flaveria*. *J. Exp. Bot.* **68**, 311 (2017).
27. S. D. Gupta et al., The C4Ppc promoters of many C4 grass species share a common regulatory mechanism for gene expression in the mesophyll cell. *Plant J.* **101**, 204–216 (2020).
28. X. Tu et al., Limited conservation in cross-species comparison of GLK transcription factor binding suggested wide-spread cistrome divergence. *Nat. Commun.* **13**, 7632 (2022).
29. M. H. Dai et al., Chromatin and regulatory differentiation between bundle sheath and mesophyll cells in maize. *Plant J.* **109**, 675–692 (2022).
30. D. A. Cusanovich et al., A single-cell atlas of in vivo mammalian chromatin accessibility. *Cell* **174**, 1309–1324.e18 (2018).
31. D. M. Emms, S. Kelly, OrthoFinder: Phylogenetic orthology inference for comparative genomics. *Genome Biol.* **20**, 238 (2019).
32. M. Taniguchi, T. Sugiyama, The expression of 2-oxoglutarate/malate translocator in the bundle-sheath mitochondria of *Panicum miliaceum*, a NAD-malic enzyme-type C4 plant, is regulated by light and development. *Plant Physiol.* **114**, 285–293 (1997).

33. Y. Taniguchi *et al.*, Differentiation of dicarboxylate transporters in mesophyll and bundle sheath chloroplasts of maize. *Plant Cell Physiol.* **45**, 187–200 (2004).
34. S. L. Tauta *et al.*, Developmental dynamics of Kranz cell transcriptional specificity in maize leaf reveals early onset of C4-related processes. *J. Exp. Bot.* **65**, 3543–3555 (2014).
35. A. R. Borba *et al.*, Compartmentation of photosynthesis gene expression in C4 maize depends on time of day. *Plant Physiol.* **193**, 2306–2320 (2023).
36. S. Weissmann *et al.*, DCT4—A new member of the dicarboxylate transporter family in C4 grasses. *Genome Biol.* **13**, evaa251 (2021).
37. M. Nomura *et al.*, The promoter for C4-type mitochondrial aspartate aminotransferase does not direct bundle sheath-specific expression in transgenic rice plants. *Plant Cell Physiol.* **46**, 743–753 (2005).
38. M. Taniguchi, A. Kobe, M. Kato, T. Sugiyama, Aspartate aminotransferase isozymes in *Panicum miliaceum* L., an NAD-malic enzyme-type C4 plant: Comparison of enzymatic properties, primary structures, and expression patterns. *Arch. Biochem. Biophys.* **318**, 295–306 (1995).
39. M. Taniguchi, H. Sawaki, H. Sasakawa, T. Hase, T. Sugiyama, Cloning and sequence analysis of cDNA encoding aspartate aminotransferase isozymes from *Panicum miliaceum* L., a C4 plant. *Eur. J. Biochem.* **204**, 611–620 (1992).
40. D. Son, J. Jo, T. Sugiyama, Purification and characterization of alanine aminotransferase from *Panicum miliaceum* leaves. *Arch. Biochem. Biophys.* **289**, 262–266 (1991).
41. T. Furumoto *et al.*, A plastidial sodium-dependent pyruvate transporter. *Nature* **476**, 472–475 (2011).
42. Y. Wang, A. Bräutigam, A. P. M. Weber, X. G. Zhu, Three distinct biochemical subtypes of C4 photosynthesis? A modelling analysis. *J. Exp. Bot.* **65**, 3567–3578 (2014).
43. C. Zou *et al.*, The genome of broomcorn millet. *Nat. Commun.* **10**, 436 (2019).
44. J. D. Washburn *et al.*, Distinct C4 sub-types and C3 bundle sheath isolation in the Paniceae grasses. *Plant Direct.* **5**, e373 (2021).
45. C. Engineer *et al.*, CO₂ sensing and CO₂ regulation of stomatal conductance: Advances and open questions. *Trends Plant Sci.* **21**, 16–30 (2016).
46. K. C. Bansal *et al.*, Transient expression from cab-m1 and rbcS-m3 promoter sequences is different in mesophyll and bundle sheath cells in maize leaves. *Proc. Natl. Acad. Sci. U.S.A.* **89**, 3654–3658 (1992).
47. J. F. Viret, Y. Mabrouk, L. Bogorad, Transcriptional photoregulation of cell-type-preferred expression of maize rbcS-m3: 3' and 5' sequences are involved. *Proc. Natl. Acad. Sci. U.S.A.* **91**, 8577–8581 (1994).
48. Z. Lu *et al.*, The prevalence, evolution and chromatin signatures of plant regulatory elements. *Nat. Plants* **5**, 1250–1259 (2019).
49. M. Taniguchi *et al.*, The promoter for the maize C4 pyruvate, orthophosphate dikinase gene directs cell- and tissue-specific transcription in transgenic maize plants. *Plant Cell Physiol.* **41**, 42–48 (2000).
50. L. Heimann *et al.*, A common histone modification code on C4 genes in maize and its conservation in *Sorghum* and *Setaria italica*. *Plant Physiol.* **162**, 456–469 (2013).
51. A. H. Paterson *et al.*, The *Sorghum bicolor* genome and the diversification of grasses. *Nature* **457**, 551–556 (2009).
52. K. A. Maher *et al.*, Profiling of accessible chromatin regions across multiple plant species and cell types reveals common gene regulatory principles and new control modules. *Plant Cell* **30**, 15–36 (2018).
53. S. Yanagisawa, Dof1 and Dof2 transcription factors are associated with expression of multiple genes involved in carbon metabolism in maize. *Plant J.* **21**, 281–288 (2000).
54. R. Perduns, I. Horst-Niessen, C. Peterhansel, Photosynthetic genes and genes associated with the C4 trait in maize are characterized by a unique class of highly regulated histone acetylation peaks on upstream promoters. *Plant Physiol.* **168**, 1378–1388 (2015).
55. D. M. Emms, S. Covshoff, J. M. Hibberd, S. Kelly, Independent and parallel evolution of new genes by gene duplication in two origins of C4 photosynthesis provides new insight into the mechanism of phloem loading in C4 species. *Mol. Biol. Evol.* **33**, 1796–1806 (2016).
56. H. Yan *et al.*, Evolution of cell-type-specific accessible chromatin regions and the cis-regulatory elements that drive lineage-specific innovation [Internet]. bioRxiv [Preprint] (2024). <https://www.biorxiv.org/content/10.1101/2024.01.08.574753v1> (Accessed 9 January 2024).
57. J. Swift *et al.*, Single nuclei sequencing reveals C4 photosynthesis is based on rewiring of ancestral cell identity networks [Internet]. bioRxiv [Preprint] (2023). <https://www.biorxiv.org/content/10.1101/2023.10.26.562893v1> (Accessed 27 October 2023).
58. A. J. Studer *et al.*, The draft genome of the C3 panicoid grass species *Dichanthelium oligosanthes*. *Genome Biol.* **17**, 223 (2016).
59. Z. Chen, J. M. Debernardi, J. Dubcovsky, A. Gallavotti, The combination of morphogenic regulators BABY BOOM and GRF-GIF improves maize transformation efficiency [Internet]. *Plant Biol.* (2022), <http://biorxiv.org/lookup/doi/10.1101/2022.09.02.506370>. Accessed 1 February 2024.
60. D. Ciren, S. Zebell, Z. B. Lippman, Extreme restructuring of cis-regulatory regions controlling a deeply conserved plant stem cell regulator [Internet]. bioRxiv [Preprint] (2023). <https://www.biorxiv.org/content/10.1101/2023.12.20.572500v1> (Accessed 2 January 2024).
61. L. Liu *et al.*, Enhancing grain-yield-related traits by CRISPR-Cas9 promoter editing of maize CLE genes. *Nat. Plants* **7**, 287–294 (2021).
62. D. Rodriguez-Leal, Z. H. Lemmon, J. Man, M. E. Bartlett, Z. B. Lippman, Engineering quantitative trait variation for crop improvement by genome editing. *Cell* **171**, 470–480.e8 (2017).
63. X. Tu, A. P. Marand, R. J. Schmitz, S. Zhong, A combinatorial indexing strategy for low-cost epigenomic profiling of plant single cells. *Plant Commun.* **3**, 100308 (2022).
64. M. Martin, Cutadapt removes adapter sequences from high-throughput sequencing reads. *EMBnet J.* **17**, 10–12 (2011).
65. H. Li, R. Durbin, Fast and accurate short read alignment with Burrows-Wheeler transform. *Bioinformatics* **25**, 1754–1760 (2009).
66. P. Danecek *et al.*, Twelve years of SAMtools and BCFtools. *GigaScience* **10**, giab008 (2021).
67. Picard Tools, By Broad Institute [Internet]. <http://broadinstitute.github.io/picard/>. Accessed 4 January 2024.
68. L. McInnes, J. Healy, J. Melville, UMAP: Uniform manifold approximation and projection for dimension reduction [Internet]. arXiv [Preprint] (2020). <http://arxiv.org/abs/1802.03426>. Accessed 19 December 2022.
69. S. L. Wolock, R. Lopez, A. M. Klein, Scrublet: Computational identification of cell doublets in single-cell transcriptomic data. *Cell Syst.* **8**, 281–291.e9 (2019).
70. I. Korsunsky *et al.*, Fast, sensitive and accurate integration of single-cell data with Harmony. *Nat. Methods* **16**, 1289–1296 (2019).
71. I. Korsunsky, A. Nathan, N. Millard, S. Raychaudhuri, Presto scales Wilcoxon and auROC analyses to millions of observations [Internet]. *Bioinformatics* (2019), <http://biorxiv.org/lookup/doi/10.1101/653253>. Accessed 28 December 2023.
72. K. Zhang *et al.*, A single-cell atlas of chromatin accessibility in the human genome. *Cell* **184**, 5985–6001.e19 (2021).
73. S. Zhong, C3 C4 grasses single-cell ATAC-seq (ID 1063172). BioProject - NCBI. <https://www.ncbi.nlm.nih.gov/bioproject?term=PRJNA1063172>. Deposited 24 January 2023.
74. R. J. Schmitz, Rice single-cell ATAC-seq (ID 1007577). BioProject - NCBI. <https://www.ncbi.nlm.nih.gov/bioproject?term=PRJNA1063172>. Deposited 9 September 2023.
75. J. P. Mendieta, Jome0169/Mendieta.C4_manuscript. GitHub. https://github.com/Jome0169/Mendieta.C4_manuscript. Deposited 1 September 2024.
76. R. J. Schmitz, PlantEpigenome. PlantEpigenome. <https://epigenome.genetics.uga.edu/PlantEpigenome/>. Deposited 9 September 2023.